Theoret. Chim. Acta (Berl.) 64, 319–338 (1984)

THEORETICA CHIMICA ACTA

Original Investigations

Reaction potential map analysis of chemical reactivity—III

Site selectivity in SCN^-, OCN^-, NO_2^-, and CH_2CHO^- anions

Hideki Moriishi, Osamu Kikuchi,* and Keizo Suzuki

Department of Chemistry, The University of Tsukuba, Sakura, Ibaraki 305, Japan

Gilles Klopman*

Department of Chemistry, Case Western Reserve University, Cleveland, Ohio 44106, USA

Reaction potential maps (RPM) have been introduced as a new tool for the study of molecular reactivity. The equipotential energy maps, which are created on given planes around a molecule, define reaction contours towards specific counter-reagent models and are evaluated by perturbation theory. Since the calculated interaction energy involves electrostatic, polarization, exchange, and charge transfer energies, the RPM's can be used to predict site selectivity in a variety of chemical reactions. We found that the calculated RPM's of the SCN^- anion explained well the experimental observations that it reacts at the S atom with soft electrophiles and at the N atom with hard electrophiles. The difference in reactivity between SCN^- and OCN^- was clearly shown by the RPM's of these anions. The ambident nucleophilic nature of the NO_2^- and the CH_2CHO^- anions was also well represented by their RPM's.

Key words: Reaction potential map—Reactivity—Ambident anions—SCN^-—OCN^-—NO_2^-—CH_2CHO^-

1. Introduction

The calculation of electrostatic potential maps (EPM) as a guide to the reactive regions of molecules was pioneered by Bonaccorsi et al. [1]. The construction of

* Authors to whom reprint requests and correspondence should be addressed

the equipotential maps is based on the value of the electrostatic potentials calculated for all points surrounding a molecule. Thus, for a given electron density function $\rho(q)$ and a set of nuclear charges, Z_α, the electrostatic potential at a given point p is expressed by:

$$V(p) = \sum_\alpha \frac{Z_\alpha}{R_{p\alpha}} - \int \frac{\rho(q)}{R_{pq}} dq. \tag{1}$$

The presence of negative potential wells is associated with possible locations of an approaching cation and the method is therefore suitable for evaluating chemical reaction paths.

EPM's were quickly adopted as a major tool for the elucidation of the reactive properties of molecules [2]. The chemical interactions and reactions of biological compounds [3–9], protonation of radical anions [10], aromatic substitution reactions [11–13], and excited state reactivity [14, 15] have all been analyzed by this technique.

Although EPM's have been very successful, particularly in the above studies of protonation reactions, their general applicability remain somewhat limited due to the fact that they only involve electrostatic interactions and that orbital symmetry factors are not included in the calculations. It is not surprising, therefore, to find that the method fails in studies of nucleophilic reactivity, where such interactions are often very important. Another shortcoming is that the methodology does not account for the nature of the reagent. Thus it cannot be used to study ambident species, i.e. species that react at different sites depending on the electronic property of the counter reagent.

For these reasons, we have undertaken a reevaluation of the procedure and proposed a method, called Reaction Potential Map (RPM), which is designed to improve the breadth of application of this technology.

Previous studies have shown that the total interaction energy between two reagents consists not only of electrostatic terms, but includes polarization, exchange, charge transfer, and dispersion components as well [16, 17]. One possible improvement in the evaluation of EPM consists in the introduction of the polarization of the molecule by the approaching proton. This has been done in the literature through a perturbation treatment that brings the excited configurations of the molecule into consideration [18–21]. However, it is now accepted that charge transfer interactions are even more important during the reaction process, and to explain the experimentally observed site selectivity, it seemed necessary to consider not only the charge (electrostatic), but also the orbital (charge transfer) interaction terms [22–27].

The Reaction Potential Maps (RPM's) are created by calculating such terms for the interaction between the molecule to be investigated and a model reagent successively placed at all points in space. Although the model reagent may, in principle, be an electrophile, a nucleophile, or a radical, the current implementation deals only with the former type of reagent. The use of a model reagent as

the counter reagent, rather than a specific molecule, simplifies the calculation enormously, but will only generate a qualitative, but hopefully general, trend of the chemical reactivity of the molecule. In this paper, the interaction energy is evaluated by the perturbation equations for interacting system [28–30]. The electron density functions of the various molecules were evaluated from CNDO/2 [31] wavefunctions. On the other hand, most intermolecular interaction terms were calculated exactly from Slater atomic orbitals. The new methodology was applied to the elucidation of the reaction sites of the SCN^- [32], OCN^-, NO_2^-, and CH_2CHO^- anions.

2. Perturbation theory

The simple equations for the interaction energy calculation between two molecules have been given by Klopman [24] and Salem [25]. Although these equations were derived with some drastic approximations, their simple forms give nice insight into the mechanics of chemical reactions, and they are widely used by organic chemists [33, 34]. In the present study, we have adopted a more rigorous intermolecular perturbation theory proposed by Murrell et al. [28–30] and describe its implementation for the evaluation of the Reaction Potential Map.

The following notations are used for the interaction between two closed-shell molecules A and B.

a_i: occupied molecular orbitals of A.

a_k: unoccupied molecular orbitals of A.

b_j: occupied molecular orbitals of B.

b_l: unoccupied molecular orbitals of B.

χ_r, χ_s: atomic orbitals in A.

α, β: core atoms in $A(\alpha)$ and $B(\beta)$.

μ, ν: electrons in $A(\mu)$ and $B(\nu)$.

The intermolecular potential U is expressed by:

$$U = -\sum_{\nu}\sum_{\alpha} \frac{Z_\alpha e^2}{r_{\nu\alpha}} - \sum_{\mu}\sum_{\beta} \frac{Z_\beta e^2}{r_{\mu\beta}} + \sum_{\mu}\sum_{\nu} \frac{e^2}{r_{\mu\nu}} + \sum_{\alpha}\sum_{\beta} \frac{Z_\alpha Z_\beta e^2}{R_{\alpha\beta}}. \tag{2}$$

The wavefunction of the interacting A–B system is represented by the linear combination of the determinantal wavefunctions constructed from the molecular orbitals of A and B in their isolated states

$$\psi = C_0\psi_0 + \sum_p C_p\psi_p. \tag{3}$$

ψ_p are the wavefunctions corresponding to the excited electron configurations, and the zeroth order wavefunction, ψ_0, is given by the following anti-symmetrical

determinant

$$\psi_0 = |a_1\bar{a}_1 \ldots a_i\bar{a}_i \ldots b_1\bar{b}_1 \ldots b_j\bar{b}_j \ldots|. \tag{4}$$

The interaction energy is expanded as a power series in the intermolecular potential U and the overlap S up to order of U^2S^2, as given by Murell et al. [28]. Among the excited configurations, ψ_p, only the $a_i \rightarrow a_k$ and $b_j \rightarrow b_l$ types of one-electron excited configurations and the $a_i \rightarrow b_l$ and $b_j \rightarrow a_k$ types of one-electron transfer configurations were taken into account. In this case, the interaction energy is expressed in molecular orbital terms as shown in Eqs. (5–12). The energy components E_Q, E_K, E_I, and E_{CT} are electrostatic, exchange, polarization, and charge transfer energies, respectively.

$$E_{int} = E_Q + E_K + E_I + E_{CT} \tag{5}$$

$$E_Q = 2\sum_i V_{ii}^B + 2\sum_j V_{jj}^A + 4\sum_{ij}\sum \langle ii|jj\rangle + \sum_{\alpha\beta}\sum Z_\alpha Z_\beta e^2/R_{\alpha\beta} \tag{6}$$

$$\begin{aligned} E_K = -2\sum_{ij}\sum \Bigg[\langle ij|ij\rangle + S_{ij} \Bigg\{ V_{ij}^B + V_{ij}^A + 2\sum_{i'} \langle ij|i'i'\rangle - \langle ij|ii\rangle \\ + 2\sum_{j'} \langle ij|j'j'\rangle - \langle ij|jj\rangle \Bigg\} - S_{ij}^2 \Bigg\{ V_{ii}^B + V_{jj}^A \\ + 2\sum_{i'} \langle jj|i'i'\rangle + 2\sum_{j'} \langle ii|j'j'\rangle - \langle ii|jj\rangle \Bigg\} \Bigg] \end{aligned} \tag{7}$$

$$\begin{aligned} E_I = 2\sum_{ik}\sum \left\{ V_{ik}^B + 2\sum_j \langle ik|jj\rangle \right\}^2 \Big/ (E_0 - E_{i\rightarrow k}) \\ + 2\sum_{jl}\sum \left\{ V_{jl}^A + 2\sum_i \langle ii|jl\rangle \right\}^2 \Big/ (E_0 - E_{j\rightarrow l}) \end{aligned} \tag{8}$$

$$\begin{aligned} E_{CT} = 2\sum_{il}\sum \left[V_{il}^B + 2\sum_j \langle il|jj\rangle - S_{il} \left\{ V_{ii}^B + 2\sum_j \langle ii|jj\rangle \right\} \right]^2 \Big/ (E_0 - E_{i\rightarrow l}) \\ + 2\sum_{jk}\sum \left[V_{jk}^A + 2\sum_i \langle ii|jk\rangle - S_{jk} \left\{ V_{jk}^A + 2\sum_i \langle ii|jj\rangle \right\} \right]^2 \Big/ (E_0 - E_{j\rightarrow k}) \end{aligned} \tag{9}$$

where

$$V_{ij}^B = -\int a_i(1) \sum_\beta \frac{Z_\beta e^2}{r_{1\beta}} b_j(1)\, d\tau_1 \tag{10}$$

$$\langle ik|jl\rangle = \iint a_i(1) a_k(1) \frac{e^2}{r_{12}} b_j(2) b_l(2)\, d\tau_1\, d\tau_2 \tag{11}$$

$$S_{ij} = \int a_i(1) b_j(1)\, d\tau_1 \tag{12}$$

2.1. Model Electrophile

The intermolecular perturbation method has previously been applied to the nucleophilic attack by OH^- on carbonyl compounds by Stone and Erskine [35].

It was found that when the interactions are calculated between two specific reagents, the orientation of the reagent with respect to the substrate is sometimes difficult to assess. We have therefore decided to model the reagents as single particles.

In the present study, dealing with ambident nucleophiles, we employed a particle consisting of a nucleus of charge +1 and an empty 1s Slater atomic orbitals. This particle can induce polarization of the substrate, and its empty 1s orbital can receive electrons from the molecule by a charge transfer mechanism. The particle's orbital energy, ε_b, is a parameter that could be related to the softness/hardness [27, 36] of the approaching reagent; i.e. soft electrophiles have low orbital energies and hard ones have a higher orbital energy. With this simplification, the perturbation Eqs. (6–9) for the nucleophile (A) – electrophile (B) system reduces to:

$$E_Q = 2\sum_i V_{ii}^B + \sum_\alpha Z_\alpha e^2/R_{\alpha\beta} \tag{13}$$

$$E_K = 0 \tag{14}$$

$$E_1 = 2\sum_i \sum_k \{V_{ik}^B\}^2/(\varepsilon_i - \varepsilon_k + \langle ii|kk\rangle - 2\langle ik|ki\rangle) \tag{15}$$

$$E_{CT} = 2\sum_i \{V_{ib}^B - S_{ib}V_{ii}^B\}^2/(\varepsilon_i - \varepsilon_b). \tag{16}$$

Eq. (13) is identical to the expression used in the calculation of the classical electrostatic potential map [1].

When the molecule to be investigated has degenerate molecular orbitals, ϕ_m and ϕ_n, the canonical forms of ϕ_m and ϕ_n are not appropriate for use in the evaluation of the charge transfer term, E_{CT}, since the contribution of these degenerate orbitals, Eq. (17), is not invariant under the arbitrary mixing of degenerate

$$E_{CT}(m, n) = 2\{V_{mb}^B - S_{mb}V_{mm}^B\}^2/(\varepsilon_m - \varepsilon_b) + 2\{V_{nb}^B - S_{nb}V_{nn}^B\}^2/(\varepsilon_n - \varepsilon_b) \tag{17}$$

orbitals. In other words, without appropriate correction, the symmetry properties of the molecule would be lost. For example, the E_{CT} map of the linear SCN^- anion calculated from Eq. (17) will not be symmetrical with respect to the rotation about the S–C–N axis. It is then necessary to perform a unitary transformation of the (ϕ_m, ϕ_n) orbitals into a set of complex orbitals (ϕ_{m^*}, ϕ_{n^*}) which are invariant with respect to the symmetry operation of the molecule. The E_{CT} term which reflects the symmetry property of the molecule is then obtained from:

$$\begin{aligned} E_{CT}(m^*, n^*) = {} & 2\{V_{mb}^B - \tfrac{1}{2}S_{mb}(V_{mm}^B + V_{nn}^B)\}^2/(\varepsilon_m - \varepsilon_b) \\ & + 2\{V_{nb}^B - \tfrac{1}{2}S_{nb}(V_{mm}^B + V_{nn}^B)\}^2/(\varepsilon_n - \varepsilon_b) \end{aligned} \tag{18}$$

which is invariant under the arbitrary mixing of the degenerate ϕ_m and ϕ_n orbitals.

2.2. Computational details

The wavefunctions of all nucleophiles were calculated by means of the CNDO/2 method [31]. The molecular orbitals, a_i, are expressed as:

$$a_i = \sum_r C_{ri}\chi_r \tag{19}$$

Since the CNDO/2 LCAO coefficients C satisfy $C^{\dagger}C = 1$ and the Slater AO set, χ, is not an orthogonal one, the molecular orbitals a_i are not normalized. This is not a serious problem as long as one deals with isolated molecules. However, in order to calculate the intermolecular interactions, it is necessary that the interacting orbitals i and b are normalized. To achieve this, we defined alternate molecular orbitals as:

$$a'_i = \sum_r C'_{ri}\chi_r \tag{20}$$

which satisfy $C'^{\dagger}SC' = 1$. The transformed coefficients, C', were obtained from appropriate transformation [37] of the CNDO/2 coefficients and from the overlap integrals S between the Slater AO basis set. They were used in the evaluation of all the intermolecular integrals.

The integrals to be evaluated can now be expanded in terms of the AO integrals as follows:

$$V^B_{ii} = \sum_{r,s} C'_{ri}C'_{si}V^B_{rs} \tag{21}$$

$$V^B_{ik} = \sum_{r,s} C'_{ri}C'_{sk}V^B_{rs} \tag{22}$$

$$V^B_{ib} = \sum_r C'_{ri}V^B_{rb} \tag{23}$$

$$S_{ib} = \sum_r C'_{ri}S_{rb} \tag{24}$$

When p and q belong to the same atom, the core attraction integrals V^B_{pq} were calculated exactly from Slater AO's, using the analytical formulae given by Roothaan [39]. When the p and q AO's belonged to different atoms, these integrals were approximated by Mulliken's formula [38]:

$$V^B_{pq} = \tfrac{1}{2}S_{pq}(V^B_{pp} + V^B_{qq}). \tag{25}$$

In order to preserve the invariance of the RPM under rotation of the coordinate axes, the V^B_{pp} integrals were calculated by using the valence s-orbital of the atom to which the p AO belongs. Finally, the overlap integrals S_{pq} were calculated from the general formulae given by Lofthus [40].

In the present study, the model electrophiles were assigned an empty 1s Slater AO whose energy measures the softness–hardness of the reagent. Two typical values were adopted for the orbital energy; 0 eV, characterizing a soft electrophile and +6 eV, a hard electrophile. Although these values do not correspond to

specific electrophiles, they are appropriate for examining the effect of the softness of the attacking electrophile on the reactivity of the nucleophilic substrates.

3. Results and discussion

3.1. Electrostatic potential maps of cyclopropane and 2-formylamino acetamide

We first examined the EPM of cyclopropane and 2-formylamino acetamide, and compared them with the *ab initio* results available in the literature [1, 4]. Figure 1 shows the EPM of cyclopropane; its overall shape is very similar to that of the *ab initio* map given in the first paper of Bonaccorsi et al. [1]. There are three potential energy minima just outside the C–C bonds and their energy, −14 kcal/mol, is in fair agreement with the *ab initio* value of −20 kcal/mol [1].

The EPM of 2-formylamino acetamide, shown in Fig. 2, is also similar to that obtained by Tomasi [2, 41] from *ab initio* calculations, although the absolute values of the potential minima at the oxygen regions are now found to be slightly larger than those obtained before.

3.2. Analysis of reaction potential maps of the SCN^- *anion*

The EPM and RPM of the SCN^- anion were already reported in a preliminary communication [32]. Here we describe them in more detail and analyze their energy components.

The absolute values of the electrostatic potentials around SCN^- (Fig. 3) are very large compared to those found for cyclopropane and 2-formylamino acetamide (Figs. 1 and 2). This is undoubtedly due to the negative charge of the SCN^- anion. Two potential wells can be seen in this map: one near the nitrogen atom, the other near the sulfur atom. The well near the nitrogen atom is the deepest, suggesting that attack at the nitrogen is the preferred path of electrophilic attack. The reaction potential map of SCN^-, as seen by a hard electrophile (Fig. 4a), is

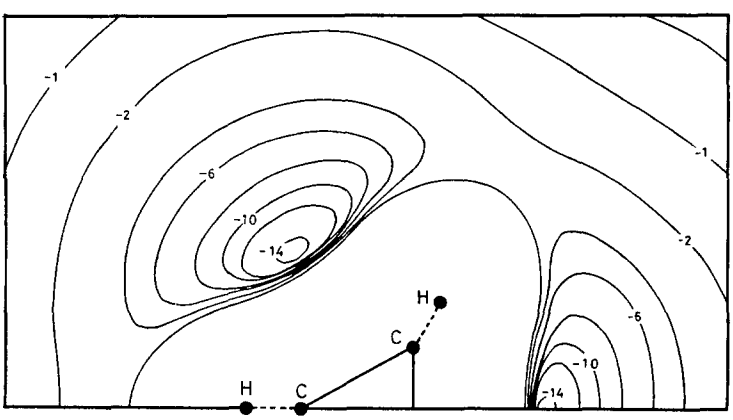

Fig. 1. Electrostatic potential map of cyclopropane on the molecular plane. The values are in kcal/mol

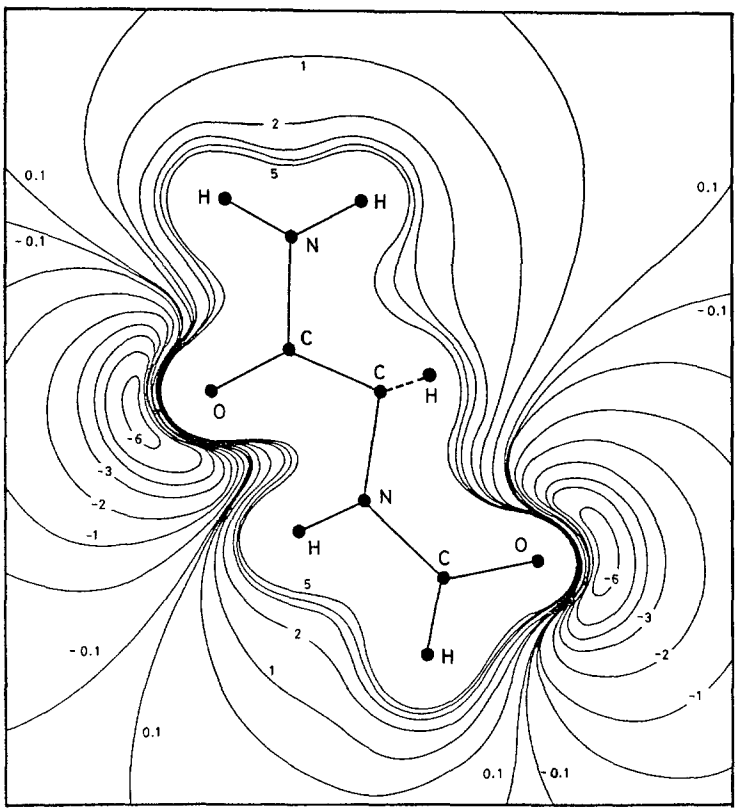

Fig. 2. Electrostatic potential map of 2-formylamino acetamide. The values are in kcal/mol

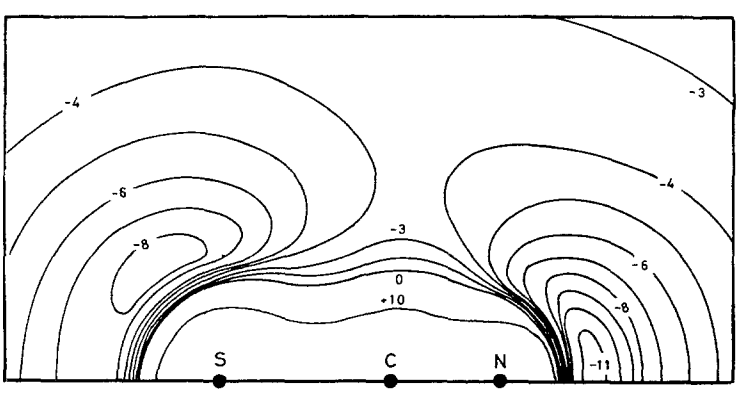

Fig. 3. Electrostatic potential map of the SCN^- anion. The values are in eV

similar to its EPM, although the minimum region near the S atom is slightly shifted. This shift is due to the existence of a charge transfer interaction between the sulfur 3p lone-pair orbitals (degenerate HOMO, Fig. 5) to the empty 1s orbital of the model electrophile. This charge transfer interaction was remarkably

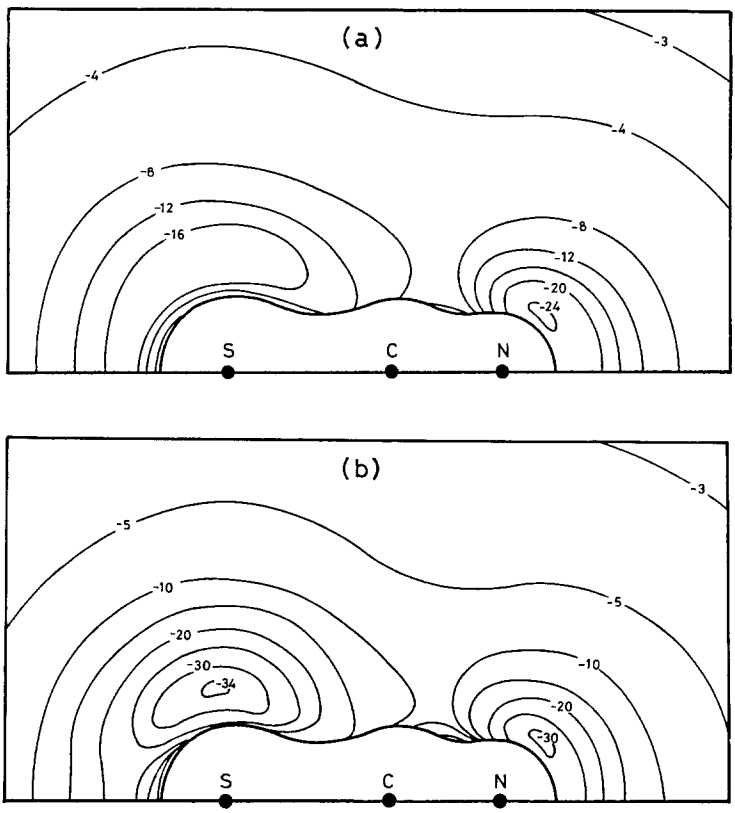

Fig. 4. Reaction potential maps of the SCN^- anion (**a**) toward the hard electrophile ($\varepsilon_b = 6$ eV), and (**b**) toward the soft electrophile ($\varepsilon_b = 0$ eV). RPM's are shown only in the area where the electrostatic potential energy is less than +10 eV. The values are in eV

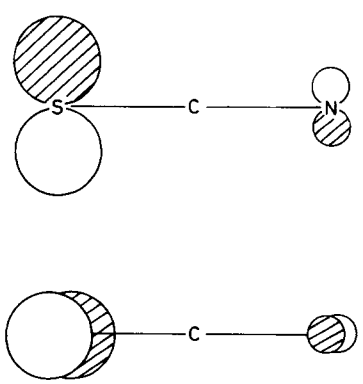

Fig. 5. The schematic shapes of the degenerate HOMO's of the SCN^- anion

0.934 -0.069 -0.349

recognized in the RPM of SCN^- as seen by a soft electrophile (Fig. 4b) and caused the potential well near the S atom to become deeper than that near the N atom. Thus the RPM's clearly show that the SCN^- anion can react at different sites depending on the softness/hardness character of the attacking electrophile.

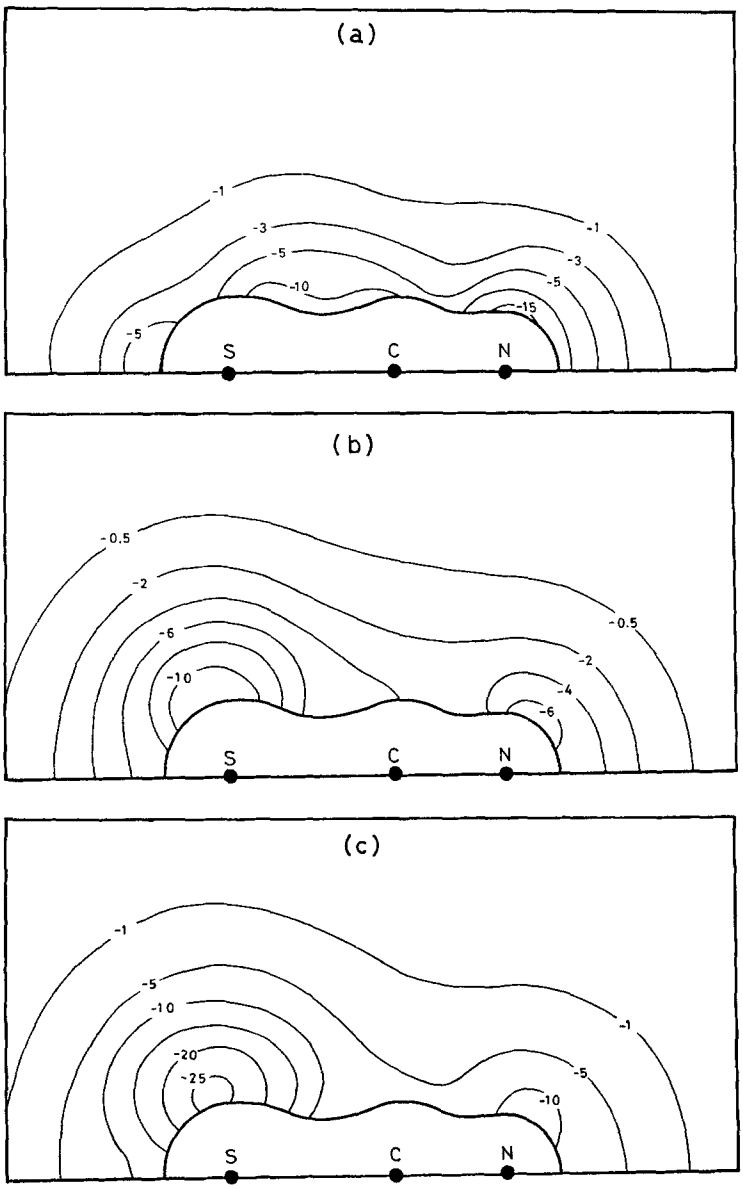

Fig. 6. Contribution of the energy components of RPM of the SCN^- anion. (**a**) Polarization energy map, (**b**) charge transfer energy map against the hard electrophile, and (**c**) charge transfer energy map against the soft electrophile. The maps are shown in the area where the electrostatic potential energy is less than +10 eV. The values are in eV

This is found experimentally [42, 43], as soft electrophiles are known to interact with the sulfur atom while hard ones prefer to react with the nitrogen atom.

The polarization and charge transfer energy components of the RPM of SCN^- are shown in Fig. 6. The polarization energy is found to be larger near the N atom than near the S atom. This is understandable since the S atom contributes only a lone-pair orbital (HOMO's in Fig. 5), while the CN group has both occupied and unoccupied polarizable π-orbitals. The charge transfer energy is basically proportional to the overlap integral, S_{ib}, between the occupied orbital i and the empty orbital of the model electrophile, ϕ_b. Since the degenerate HOMO's of SCN^- consist mainly of the sulfur 3p orbitals, the reactivity at the S center is very sensitive to the softness/hardness character of the attacking electrophile.

Fig. 7 shows more clearly the variations in the energy components of the RPM of SCN^- along a specific direction. The electrostatic energy, E_Q, is dominant at long distances even for the soft electrophile, while the charge transfer interaction, E_{CT}, increases more rapidly as the distance decreases. The contribution of each occupied MO to E_{CT} is shown in Fig. 8. As may be expected, the HOMO's contribution is the largest, and its importance increases as the softness of the electrophile increases (compare Figs. 9a and 9b).

3.3. Reactivity of the OCN^- *anion*

Although the SCN^- and OCN^- anions have the same number of valence electrons, their nucleophilic reactivities are very different. It is thus interesting to compare

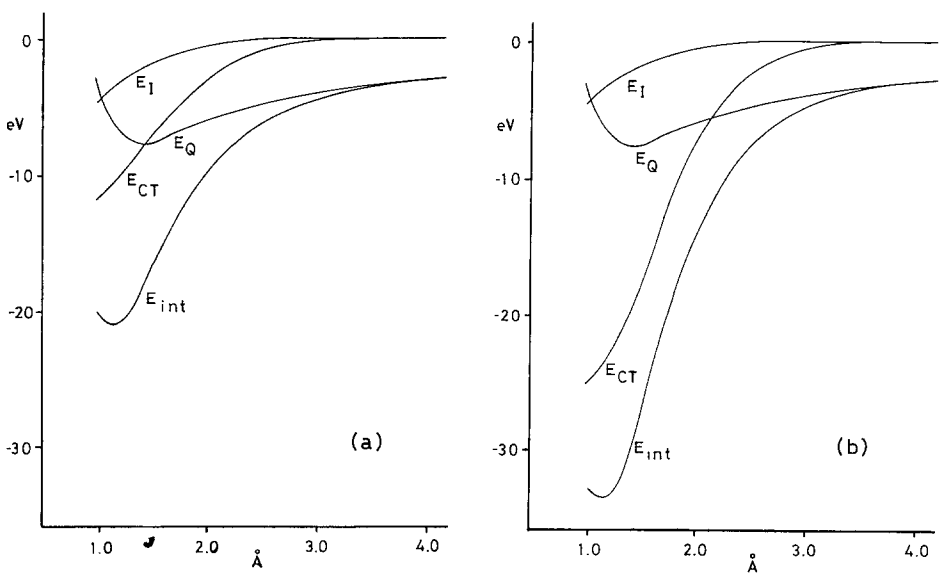

Fig. 7. Variations in the energy components of the RPM of the SCN^- anion along a specified direction. (**a**) RPM toward the hard electrophile, and (**b**) RPM toward the soft electrophile. The distance is measured from the S atom along the direction which is 95° to the S—C—N line

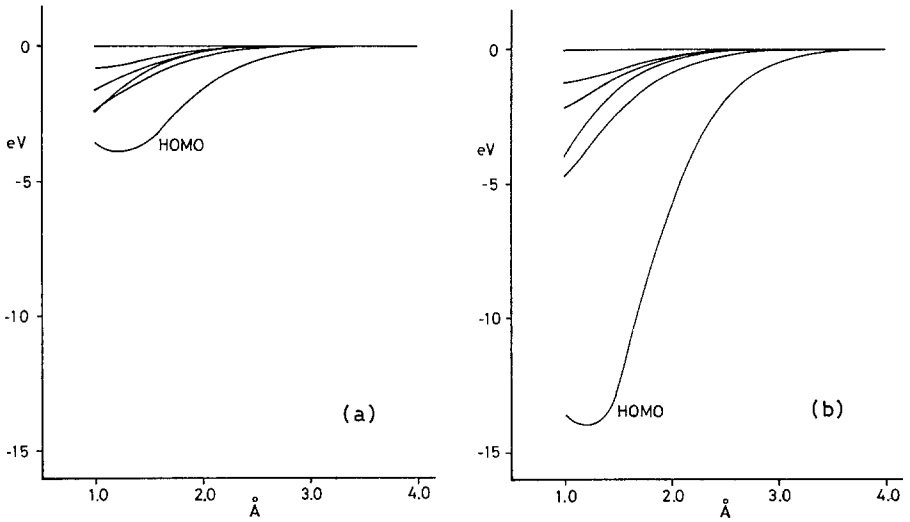

Fig. 8. Contributions of the occupied MO's to the charge transfer energy of SCN^-. (**a**) Charge transfer energy toward the hard electrophile, and (**b**) toward the soft electrophile. The distance is measured from the S atom along the direction which is 95° to the S—C—N line

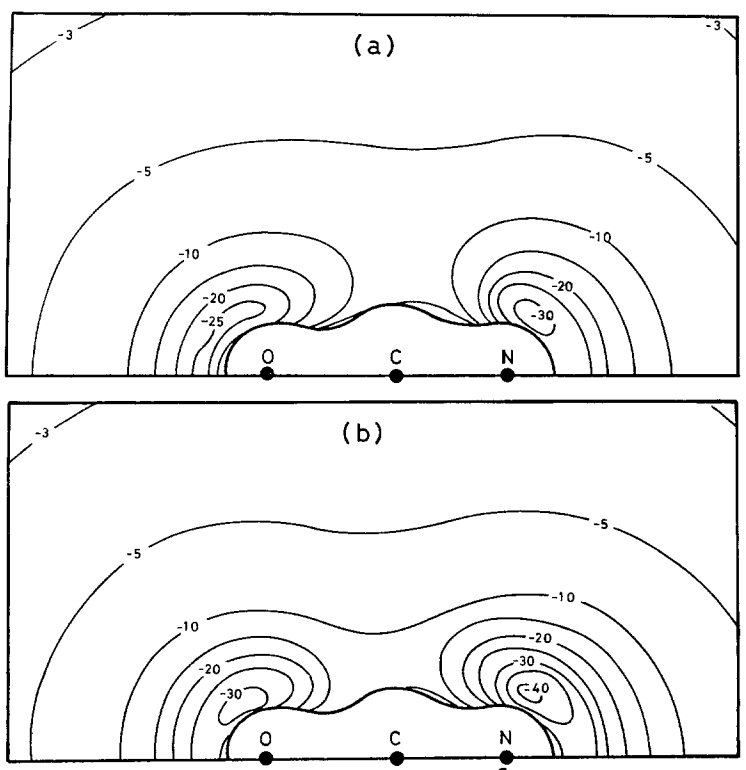

Fig. 9. Reaction potential maps of the OCN^- anion (**a**) toward the hard electrophile ($\varepsilon_b = 6$ eV) and (**b**) toward the soft electrophile ($\varepsilon_b = 0$ eV). The values are in eV

the RPM's of OCN^- with those of SCN^-. The RPM's of OCN^- toward soft and hard electrophiles are shown in Fig. 9. It can be seen that the potential well near the N atom is largely unaffected by the incoming electrophile, and remain deeper than that near the O atom. This suggests that the OCN^- anion only reacts at the N center independently of the softness/hardness character of the attacking electrophiles. This is an agreement with experiments as it is found that, in contrast

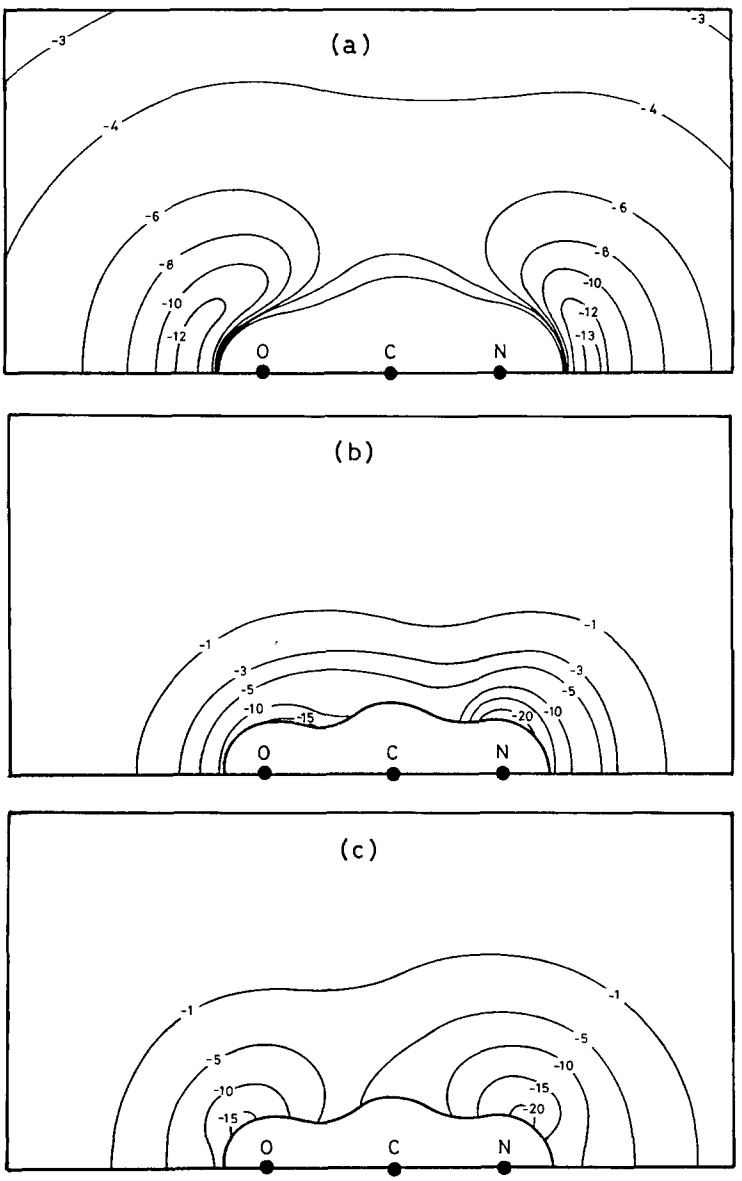

Fig. 10. Energy components of the RPM of OCN^-. (**a**) Electrostatic potential map, (**b**) polarization map, and (**c**) charge transfer energy map toward the soft electrophile. The values are in eV

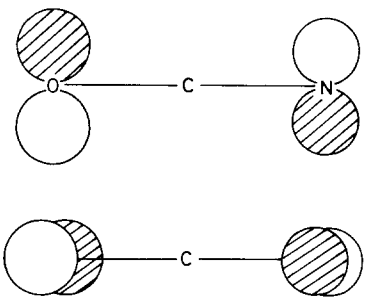

Fig. 11. The schematic shapes of the degenerate HOMO's of the OCN^- anion

to SCN^-, OCN^- reacts only with its N atom to give the isocyanate RNCO and not the isomeric cyanate ROCN [44].

Fig. 10a shows the EPM of OCN^-. Here again, two potential wells are observed and of these, that close to the nitrogen atom is deeper than that of the O region. In contrast to the previous case, though, the charge transfer term here (Fig. 10c) is also largest in the N region. This is true even for the soft electrophile and is observed in spite of the fact that the electron population of the HOMO (Fig. 11) is smaller at the N atom than at the O atom. The probable reason for this anomaly is that the nitrogen and oxygen $2p$ orbitals, having different orbital exponents, overlap differently with incoming reagents, and the overall overlap remains larger for the nitrogen than for the oxygen atom [45]. As a result, the charge transfer interaction in OCN^- is larger near the N atom even for soft electrophiles. This observation emphasizes the important fact that the magnitude of the charge transfer interaction at different kind of atoms cannot be anticipated simply from the HOMO LCAO coefficients.

3.4. The nitrous anion, NO_2^-

The RPM's of the NO_2^- anion are shown in Fig. 12. They were calculated for two planes; one is the NO_2^- molecular plane (X-plane) and the other is the Y-plane which is perpendicular to the molecular plane and bisects the ONO angle. The upper part of each RPM in Fig. 12 is the RPM on the Y-plane and

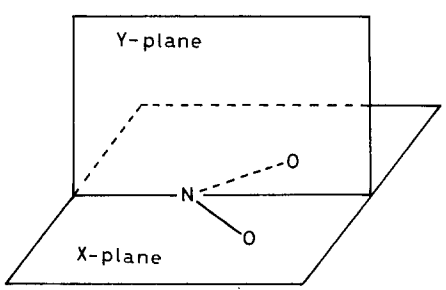

Scheme 1

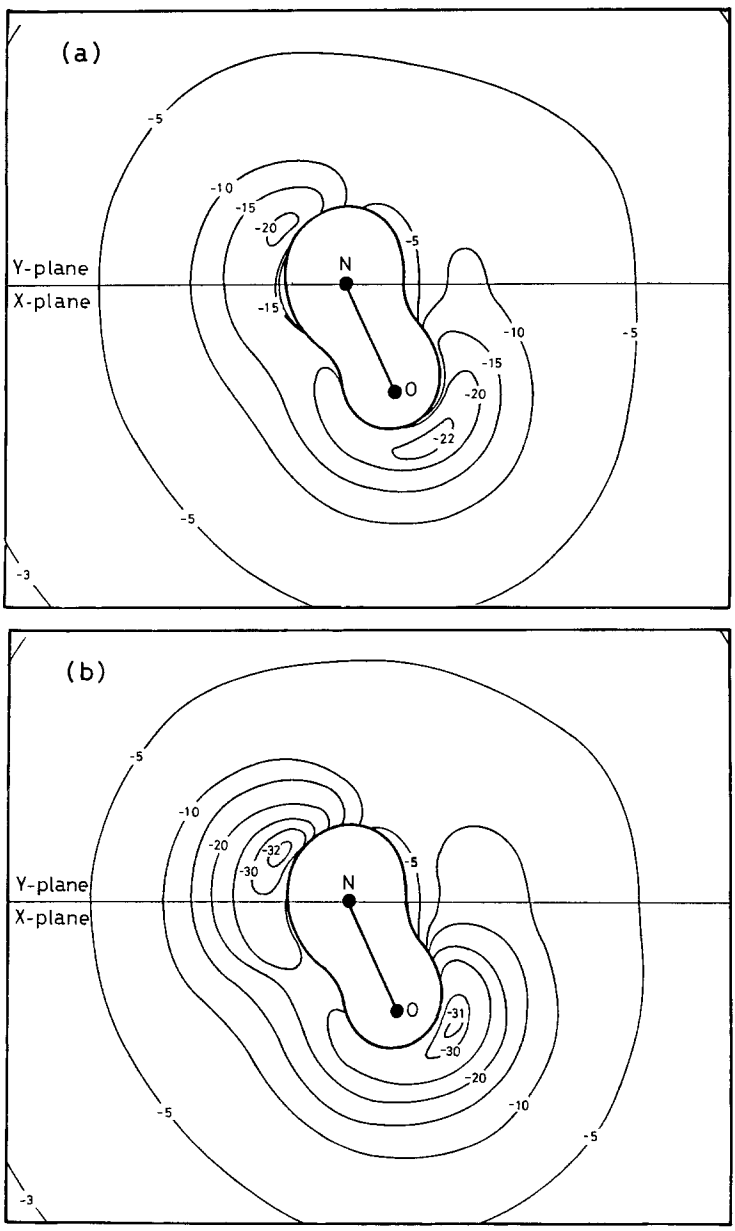

Fig. 12. Reaction potential maps of the NO_2^- anion (**a**) toward the hard electrophile and (**b**) toward the soft electrophile. The X-plane is the molecular plane and the Y-plane is perpendicular to the molecular plane and bisects the ONO angle. The values are in eV

the lower part is that on the X-plane. The deeper O region potential well observed in Fig. 12a indicates that the NO_2^- anion reacts at the O center with hard electrophiles, while the wider and deeper N region well in Fig. 12b indicates that it reacts at the N center with soft electrophiles.

The ambident nucleophilic character of NO_2^- has experimentally been observed [46, 47]. Depending on the counter ion, the reaction of nitrous salts with alkyl halides leads either to nitro derivatives or to nitrites

$$O_2NCH_2COOR \xleftarrow{Na^+} NO_2^- + BrCH_2COOR \xrightarrow{Ag^+} ONOCH_2COOR.$$

These reactions are understood as follows [27]. In the presence of a sodium ion, a hard electrophile believed to coordinate to the oxygen atoms, the soft N atom is mostly free and able to react with alkyl halides. On the other hand, a very soft counter ion such as a silver ion remains near the soft N region, and alkyl halides react at the oxygen atom.

3.5. Acetaldehyde enolate anion, CH_2CHO^-

The ambident nature of the nucleophilic character of the CH_2CHO^- anion has experimentally been observed [27, 45, 48]. The molecule reacts at the α—C atom

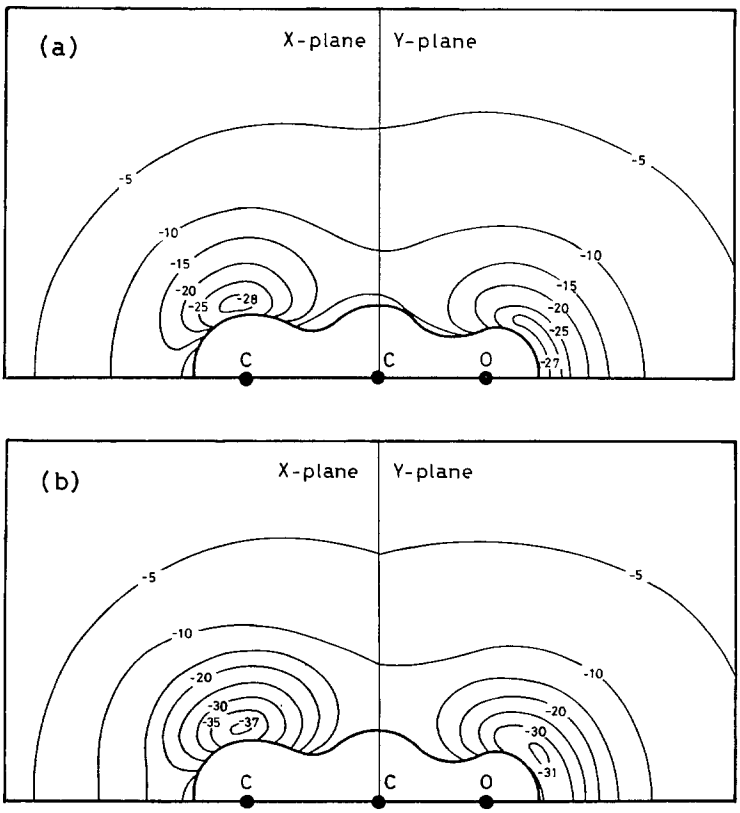

Fig. 13. Reaction potential maps of the CH_2CHO^- anion (**a**) toward the hard electrophile and (**b**) toward the soft electrophile. The *X*-plane involves the C–C bond and the *Y*-plane involves the C—O bond. Both are perpendicular to the molecular plane. The values are in eV

with the soft electrophile, CH_3Br, while reacting at the O atom with the hard electrophile, $(CH_3CH_2)_3O^+$. Fig. 13 shows the RPM's of

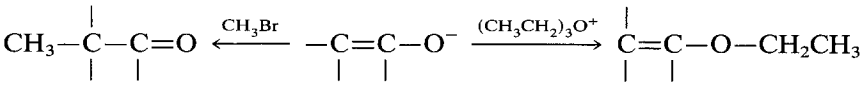

CH_2CHO^- which, again, were calculated on two planes, both perpendicular to the molecular plane; the *X*-plane intersects the molecular plane along the C—C bond while the *Y*-plane intersects it along the C—O bond. The RPM's of CH_2CHO^- show two minima; one located near the α—C atom, and the other near the O atom. In the RPM seen by a soft electrophile (Fig. 13b), the α—C region well is deeper than the O region well suggesting reaction at the carbon atom. On the other hand, in the RPM seen by a hard electrophile (Fig. 13a), the minimum energy values are comparable in the O and C regions. This suggests

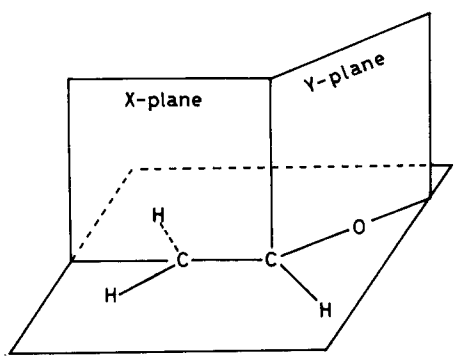

Scheme 2

that the CH_2CHO^- anion is possibly attacked by soft electrophiles at the α—C atom, while the interaction with hard electrophiles might possibly take place in either the carbon or the oxygen atom. The RPM's of CH_2CHO^- thus reflect the experimentally observed ambident behavior of CH_2CHO^-.

3.6. Ab initio STO-3G *calculation*

In order to examine the validity of the present RPM's, obtained from CNDO/2 wavefunctions, the STO-3G RPM's of the SCN^- anion were also calculated. The wavefunction was obtained by using Stewart's parameters [49]. The interaction energy between SCN^- and the model electrophile was evaluated exactly from Eqs. (13–18). The results are shown in Fig. 14. The EPM (Fig. 14a), the polarization map (Fig. 14b), and the charge transfer map (Fig. 14c), all have shapes very similar to those (Figs, 3, 6a and 6c, respectively) obtained with the approximations described before. Thus the same conclusions are reached concerning the ambident nucleophilic reactivity of SCN^- whether the calculations are made with semi-empirical or *ab initio* STO-3G calculations.

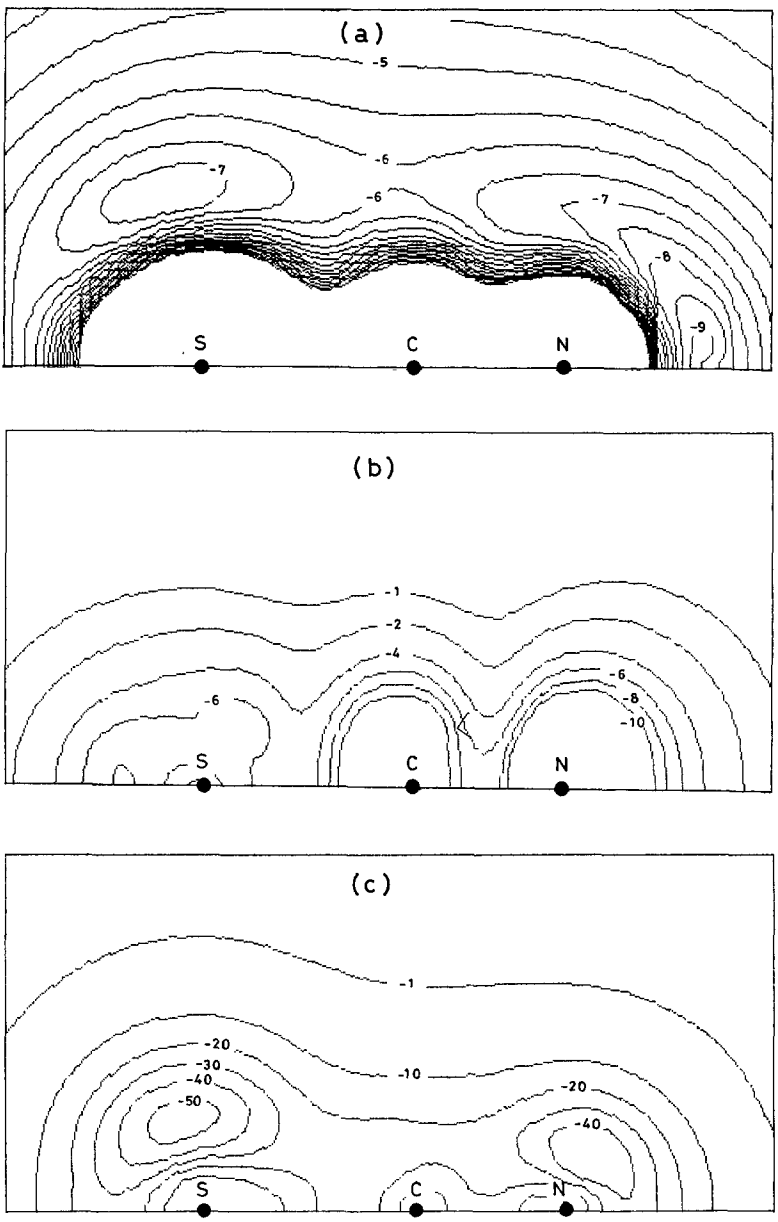

Fig. 14. *Ab initio* STO-3G maps of SCN^-. (**a**) Electrostatic potential energy map, (**b**) polarization energy map, and (**c**) charge transfer energy map. The values are in eV

4. Conclusion

The reaction potential maps reproduce the observed patterns of ambident reactivity and provide a visual means of understanding the reaction paths that lead to alternate products.

One of the problems with the methodology, as described herein, is that the potential wells are found to be much too deep to represent reactions in solution realistically. For example, even though the interaction energy between an anion and an empty orbital with a positive charge is expected to be very large, the observed wells exceed by far what should have been found, e.g. 18 eV (STO-3G) and 21.1 eV (CNDO/2) [50].

Clearly these values are unrealistic for the solution protonation of SCN^-. We believe that three factors contribute to render these values unrealistic. The first one is the fact that the solvent is not included in the calculation. The desolvation of the ions during the formation of the bond is clearly important and must contribute to decrease the energy wells. Another factor relates to perturbation theory itself and is linked to the overestimation of orbital interactions at short distances. Finally, it may be that the exchange interaction energy E_k, which is not currently involved in the RPM calculation plays an important role as well. Indeed, the exchange term is repulsive and increases rapidly with distance. These points will be addressed in a forthcoming publication.

Acknowledgments. One of us (G.K.) thanks the donors of the Petroleum Research Fund for support of this work through Grant No. PRF 14100-AC4.

References

1. Bonaccorsi, R., Scrocco, E., Tomasi, J.: J. Chem. Phys. **52**, 5270(1970)
2. Tomasi, J.: Quantum theory of chemical reactions, Daudel, R., Pullman, A., Salem, L., Veillard, A., eds. p. 191, and references cited therein. Dordrecht: Reidel 1980
3. Bonaccorsi, R., Pullman, A., Scrocco, E., Tomasi, J.: Theoret. Chim. Acta (Berl.) **24**, 51 (1972)
4. Alagona, G., Pullman, A., Scrocco, E., Tomasi, J.: Int. J. Peptide Protein Res. **5**, 251 (1973)
5. Bonaccorsi, R., Scrocco, E., Tomasi, J., Pullman, A.: Theoret. Chim. Acta (Berl.) **36**, 339 (1975)
6. Alagona, G., Scrocco, E., Tomasi, J.: J. Am. Chem. Soc. **97**, 6976 (1975)
7. Politzer, P., Daiker, K. C.: Int. J. Quantum Chem., Quant. Biol. Symp. **4**, 317 (1977)
8. Perahia, D., Pullman, A.: Theoret. Chim. Acta (Berl.) **48**, 263 (1978)
9. Hariharan, P. C., Kaufman, J., Petrongolo, C.: Int. J. Quantum Chem., Quant. Biol. Symp. **6**, 224 (1979)
10. Cremaschi, P., Gamba, A., Simmonetta, M.: Theoret. Chim. Acta (Berl.) **40**, 303 (1975)
11. Politzer, P., Donnelly, R. A., Daiker, C. K.: J. Chem. Soc. Chem. Comm. 617 (1973)
12. Politzer, P., Weinstein, H.: Tetrahedron **31**, 915 (1975)
13. Bertran, J., Silla, E., Carbo, R., Martin, M.: Chem. Phys. Letters **31**, 267 (1975)
14. Bonaccorsi, R., Scrocco, E., Tomasi, J.: Chemical and biochemical reactivity, Bergmann, E. D., Pullman, B., eds. p. 387. Jerusalem: Israel Acad. Sci. & Humanities, 1974
15. Daudel, R., Le Rouzo, H., Cimiraglia, R., Tomasi, J.: Int. J. Quantum Chem. **13**, 537 (1978)
16. Dreyfus, M., Pullman, A.: Theoret. Chim. Acta (Berl.) **19**, 20 (1970)
17. Morokuma, K.: J. Chem. Phys. **55**, 1236 (1971)
18. Bartlett, R. J., Weinstein, H.: Chem. Phys. Letters **30**, 441 (1975)
19. Bertram, J., Silla, E., Fernandez-Alonso, J. I.: Tetrahedron **31**, 1093 (1975)
20. Van der Neut, R. N.: Tetrahedron **31**, 2547 (1975)
21. Weinstein, H., Chou, D., Kang, S., Johnson, C. L., Green, J. P.: Int. J. Quantum Chem., Quant. Biol. Symp. **3**, 135 (1976)

22. Fukui, K., Yonezawa, T., Shingu, H.: J. Chem. Phys. **20**, 722 (1952)
23. Hudson, H., Klopman, G.: Tetrahedron Letters 1103 (1967)
24. Klopman, G.: J. Am. Chem. Soc. **90**, 273 (1968)
25. Salem, L.: J. Am. Chem. Soc. **90**, 543 (1968)
26. Fujimoto, H., Fukui, K.: Chemical reactivity and reaction paths, Klopman, G. ed. p. 23. New York: Wiley, 1974
27. Klopman, G.: Chemical reactivity and reaction paths, p. 55. New York: Wiley, 1974
28. Murrell, J. N., Randic, M., Williams, D. R.: Proc. Roy. Soc. **A284**, 566 (1965)
29. Murrell, J. N., Shaw, G.: J. Chem. Phys. **46**, 1768 (1967)
30. Nagase, S., Fueno, T.: Theor. Chim. Acta (Berl.) **35**, 217 (1974)
31. Pople, J. A., Segal, G. A.: J. Chem. Phys. **44**, 3289 (1966); Santry, D. P., J. Am. Chem. Soc. **90**, 3309 (1968)
32. Klopman, G., Moriishi, H., Kikuchi, O., Suzuki, K.: Tetrahedron Letters **23**, 1027 (1982)
33. Fleming, I.: Frontier orbitals and organic chemical reactions. New York: Wiley, 1976
34. Ho, T.: Hard and soft acids and bases principle in organic chemistry. New York: Academic Press, 1977
35. Stone, A. J., Erskine, R. W.: J. Am. Chem. Soc. **102**, 7185 (1980)
36. Pearson, R. G.: J. Am. Chem. Soc. **85**, 3533 (1963)
37. Löwdin, P. O.: J. Chem. Phys. **18**, 365 (1950)
38. Mulliken, R. S.: J. Chim. Phys. **46**, 521 (1949)
39. Roothaan, C. C. J., J. Chem. Phys. **19**, 1445 (1951)
40. Lofthus, A.: Mol. Phys. **5**, 105 (1962)
41. Bonaccorsi, R., Scrocco, E., Tomasi, J.: J. Am. Chem. Soc. **99**, 4546 (1977)
42. Pearson, R. G., Songstad, J.: J. Am. Chem. Soc. **89**, 1827 (1967)
43. Giles, D. E., Parker, A. J.: Aust. J. Chem. **26**, 273 (1973)
44. March, J.: Advanced organic chemistry: Reaction mechanism and structure, p. 298. New York: McGraw-Hill, 1968
45. The same conclusion was obtained by the analysis of the STO-3G RPM's of SCN^- and OCN^-
46. Hendrickson, J. A., Cram, D. J., Hammond, G. S.: Organic chemistry, p. 394, New York: McGraw-Hill, 1970
47. Kornblum, N., Smiley, R. A., Blackwood, R. K., Iffland, D. C.: J. Am. Chem. Soc. **77**, 6269 (1955)
48. Guibè, F., Sarthou, P., Bram, G.: Tetrahedron **30**, 3139 (1974)
49. Stewart, R. F.: J. Chem. Phys. **52**, 431 (1970)
50. The energies of SCN^- and SCNH were calculated for their optimized structures

Received August 1, 1983